Alexandria Engineering Journal 111 (2025) 160–170

Contents lists available at ScienceDirect

Alexandria Engineering Journal

journal homepage: www.elsevier.com/locate/aej

Keller-box based computational investigation of magnetized gravity-driven Micropolar nanofluid flow past an exponentially contracting surface with cross diffusion effect and engineering applications

Marouan Kouki [a], Saira Shukat [b], Ikram Ullah [c], Mohammad Mahtab Alam [d], Ali Hasan Ali [e,f,g,*]

[a] Department of Information Systems, Faculty of Computing and Information Technology, Northern Border University, Rafha, Saudi Arabia
[b] Department of Mathematics, University of Sialkot, Sialkot 51040, Pakistan
[c] Department of Natural Sciences and Humanities, University of Engineering and Technology, Mardan 23200, Pakistan
[d] Department of Basic Medical Sciences, College of Applied Medical Science, King Khalid University, Abha 61421, Saudi Arabia
[e] Department of Business Management, Al-imam University College, 34011 Balad, Iraq
[f] Institute of Mathematics, University of Debrecen, Pf. 400, Debrecen H-4002, Hungary
[g] Technical Engineering College, Al-Ayen University, 64001, Dhi Qar, Iraq

ARTICLE INFO

Keywords:
Keller-Box Technique
Cross diffusion effects
Micropolar nanofluid
Exponentially Stretching sheet
Solar radiation

ABSTRACT

Transport of heat in combustion engines, burners and consumption of energy via nuclear explosions is remarkably effected by magnetize nanofluid and radiation. Present attempt is relevant to the current Engineering applications; as design of heat exchangers, systems of renewable energy, and Nanotechnology. Therefore, main concern of the study is explored the radiative flux in Micropolar nanofluid flow under the Lorentz force and gravity modulation. The impacts of cross diffusion is also included in flow field. The mathematical model governing the flow are transformed into ODEs via similarity variables. The Keller box approach is utilized for numerical outcomes. A comprehensive analysis of the physical parameters is carried out, and numerical outcomes are displayed in graphical and tabular form. Obtained outcomes are compared with results that have already been published and found a good match. It has been found that temperature profile and concentration profile have a direct relation against Soret and Dufour respectively. Temperature profile and concentration profile has a direct relation against Dufour and Soret effects. Thermal field grows by enhancing radiation, Brownian motion and thermophoresis parameter. Furthermore, the skin friction.increases as the inclination factor grows up, but Nusselt and Sherwood numbers decline.

1. Introduction

There are numerous uses of the boundary layer flow through a stretched surface, including the reduction of drag, grain storage, skin friction, and paper manufacture. Sakiadis [1] conducted the first inspection on flow of boundary layer across a regular solid surface with uniform velocity. The features of Lorentz force and electric field on magnetized nanomaterials toward a nonlinear stretched surface with variable thickness was explored by Daniel et al. [2]. It was found that while the electric field decreased the concentration, it increased the nanofluid's velocity and temperature. An electrically conducting nanomaterials flow over a stretched sheet with varying thickness was numerically examined by Daniel et al. [3] to determine the impacts of thermal stratification, Lorentz force, Joules heating, and dissipation. The impact flow in stagnation region of a heated porous stretching sheet past a radiative magneto Micropolar liquid was numerically investigated by Warke et al. [4]. In [5–31] some current research on flow nanofluid is mentioned.

The recent technological world, nanotechnology is one of the significant inventions, which plays a tremoundus role in industrial and engineering area. Before the important advent of tiny particles termed as nanoparticles, regular liquieds were utilized in multiple mechanism, which produced deficiencies in outcomes. The term "nanofluid" refers to the addition of solid nanoparticles like copper, silver, titanium dioxide, or aluminum oxide in a base fluid like water, oil, or glycol. The thermal efficiency of the regular fluids is increased by adding metallic nanometer-sized particles. The thermal efficiency of the nanofluids is predicted to be more prominent than that of the regular fluids. Such

* Corresponding author at: Department of Business Management, Al-imam University College, 34011 Balad, Iraq.
E-mail address: ali.hasan@science.unideb.hu (A.H. Ali).

https://doi.org/10.1016/j.aej.2024.10.003
Received 4 May 2024; Received in revised form 3 September 2024; Accepted 1 October 2024
Available online 22 October 2024

Table 1
Comparison of $-\theta'(0)$ when $\delta, S_r, \quad D_f, Nb, Nt, \lambda, \quad K, Sc, \alpha = 0 and\ \Omega = 90^0$.

Pr	*M*	*Rd*	Bidin and Nazar [57] $-\theta'(0)$	Ishak [58] $-\theta'(0)$	Present results $-\theta'(0)$
1.0	0	0	0.9548	0.9548	0.9548
2.0	0	0	1.4714	1.4714	1.4714
3.0	0	0	1.8691	1.8691	1.8690
1.0	0	1.0	0.5312	0.5312	0.5312
1.0	1.0	0	0.8611	0.8611	0.8617
1.0	1.0	1.0	0.4505	0.4505	0.4505

fluids can be used in the cooling of electronic devices, nuclear reactors, transformer cooling in vehicles, cancer therapy, the heating and cooling of energy conversion processes, etc. In an experimental research, Choi [32] discovered that adding nanoparticles improved the thermal conductance of the base fluids. Buongiorno [33] investigated the convective transportation processes in nanofluid. He designed a mathematical model to examine the Brownian movement and thermophoretic dispersion of nanoparticles in a nanofluid flow. Nanofluid flow through stretchable surface was studied by Khan and Pop [34]. Numerical and experimental analysis of the flow of nanomaterials was inspected by Alhaj et al. [35]. The studies [36–40] illustrate some recent investigations regarding nanofluid flows.

A diffusion flux that results from a temperature differential is known as the Soret effect (thermal diffusion). The Dufour effect is a reciprocal phenomenon that happens when a chemical potential gradient causes a heat flux. Both phenomena have received substantial utilization in gases, and the liquids. Farooq et al. [41] analyzed the impacts of cross diffusion on the significant model of Oldroyd-B materials. Hayat et al. [42] analyzed the same impacts in the second-grade fluid under the effect of Lorentz force in three-dimensional (3D) flow. Sardar et al. [43] accomplished analysis on the mixed convection flow of Carreau nanomaterial's on a wedge when Soret and Dufour (SD) effects were present. The effects of (SD) on radiative stretchable cylinder is examined by Shojaei et al. [44]. The diffusive flow between permeable trapezoidal enclosures studied by Al-Mudhaf et al. [45]. Meng and Li [46] disclose the features of cross diffusion phenomena on viscoelastic materials through porous vertical channels. Eid and Jamshed [47] examined Dufour impacts on Micropolar nanofluid with permeable slanted surface. Shah et al. [48] and Borah et al. [49] explored the SD effects on nanofluid by considering the second-grade and Micropolar nanofluid flow respectively. Recent studies on SD effects and heat transfer are mentioned in [50–56]. We choose Keller box method to simulate the flow due to its ability to tackle nonlinear problem, complicated geometries as well as different boundary conditions make it preferable method over other ones in fluid dynamic simulations. This method is more efficient method than other existing methods.

1.1. Novelty and motivation

Micropolar nanomaterial's flow with cross diffusion effect has crucial applications in various technological and industrial areas like converging dies, hydrology of ground water, design of heat exchangers, systems of renewable energy, and Nanotechnology etc. Furthermore in many applications like wire drawing etc. both Soret and Dufour effects are used. Therefore the literature review and applications previously mentioned inspired us to explore the flow of the Micropolar nanomaterial's towards a stretched sheet with Brownian motion and the thermophoretic impacts. The novel features of current attempt is highlighted below:

- Lorentz force is considered for more realistic applications.
- Flow in the regimes of stagnation point is very important in aerodynamics is taken here.
- The phenomena of cross diffusion is considered for the practical analysis.

Table 2
Computational data of $-\theta'(0)$, $-\phi'(0)$ and $C_{fx}(0)$.

Nb	*Nt*	*Pr*	*Sc*	*M*	*K*	*Rd*	S_r	*Df*	λ	δ	α	Ω	$-\theta'(0)$	$-\phi'(0)$	$C_{fx}(0)$
0.1	0.1	6.5	5.0	0.1	1.0	1.0	0.1	0.1	0.1	0.1	0.5	45^0	0.3257	1.7579	0.8452
0.3	0.1	6.5	5.0	0.1	1.0	1.0	0.1	0.1	0.1	0.1	0.5	45^0	0.1231	1.8333	0.8435
0.1	**0.3**	6.5	5.0	0.1	1.0	1.0	0.1	0.1	0.1	0.1	0.5	45^0	0.1404	1.8164	0.8425
0.1	0.1	**9.0**	5.0	0.1	1.0	1.0	0.1	0.1	0.1	0.1	0.5	45^0	0.1382	1.8562	0.8468
0.1	0.1	6.5	**9.0**	0.1	1.0	1.0	0.1	0.1	0.1	0.1	0.5	45^0	−0.5131	3.2597	0.8490
0.1	0.1	6.5	5.0	**0.3**	1.0	1.0	0.1	0.1	0.1	0.1	0.5	45^0	0.3219	1.7514	0.9086
0.1	0.1	6.5	5.0	0.1	**3.0**	1.0	0.1	0.1	0.1	0.1	0.5	45^0	0.3392	1.7858	1.1116
0.1	0.1	6.5	5.0	0.1	1.0	**3.0**	0.1	0.1	0.1	0.1	0.5	45^0	−0.1003	1.8731	0.8349
0.1	0.1	6.5	5.0	0.1	1.0	1.0	**0.5**	0.1	0.1	0.1	0.5	45^0	1.0610	0.4176	0.8344
0.1	0.1	6.5	5.0	0.1	1.0	1.0	0.1	**0.3**	0.1	0.1	0.5	45^0	2.8577	−0.0262	0.8974
0.1	0.1	6.5	5.0	0.1	1.0	1.0	0.1	0.1	**0.3**	0.1	0.5	45^0	0.3285	1.7636	0.7741
0.1	0.1	6.5	5.0	0.1	1.0	1.0	0.1	0.1	0.1	**0.9**	0.5	45^0	0.3308	1.7696	0.6685
0.1	0.1	6.5	5.0	0.1	1.0	1.0	0.1	0.1	0.1	0.1	**0.7**	45^0	0.3473	1.7941	0.5351
0.1	0.1	6.5	5.0	0.1	1.0	1.0	0.1	0.1	0.1	0.1	0.5	$\boldsymbol{60^0}$	0.3251	1.7567	0.8622

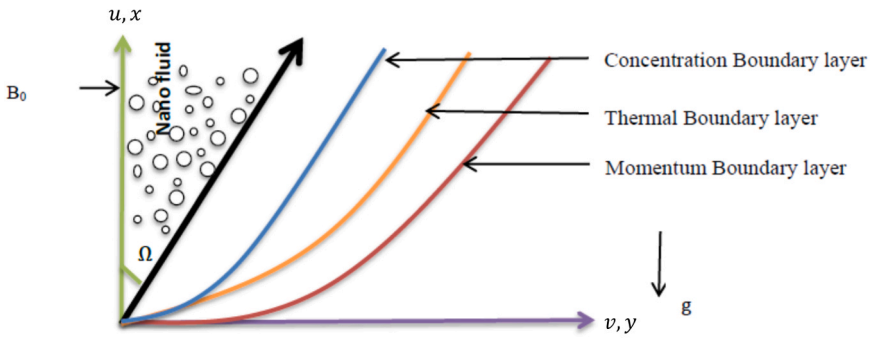

Fig. 1a. : Graphical view of considered model.

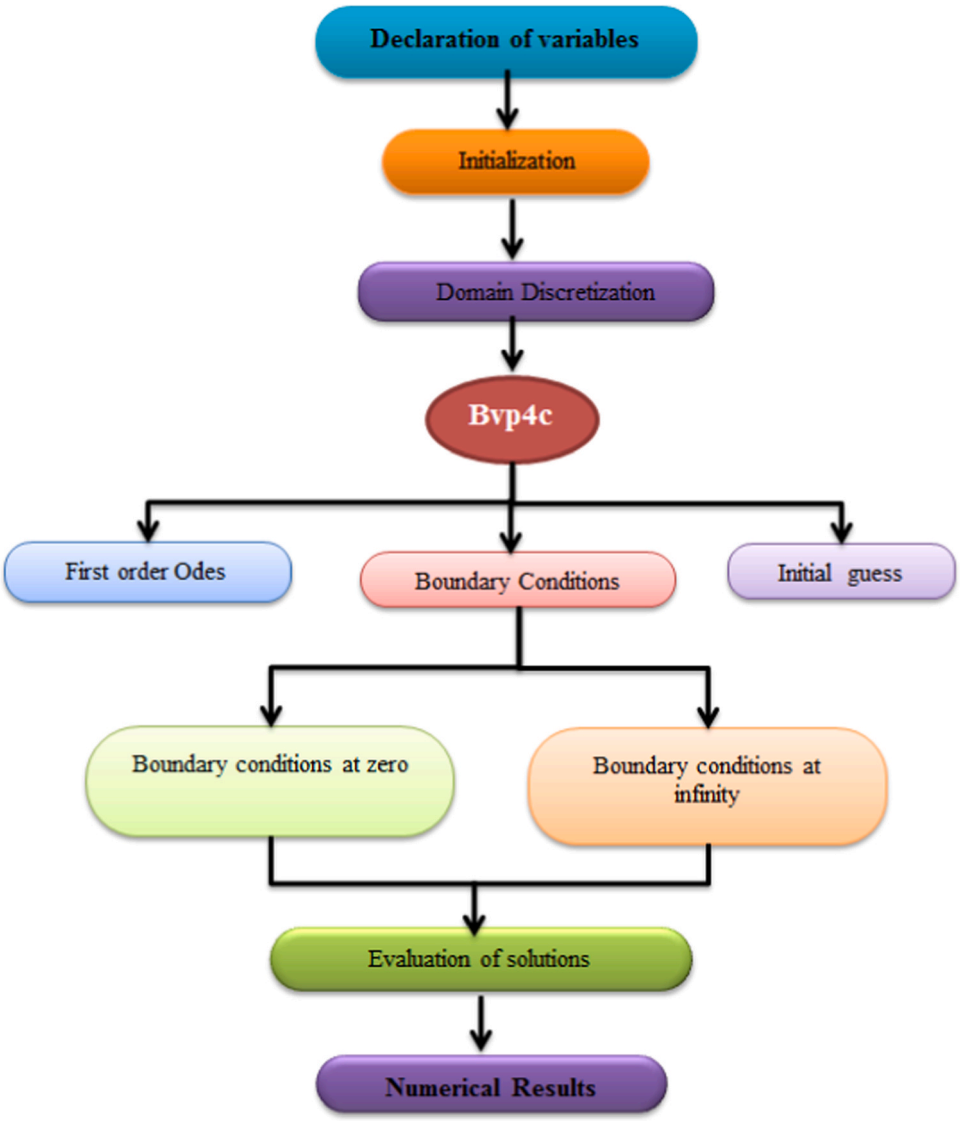

Fig. 1b. Flow chart.

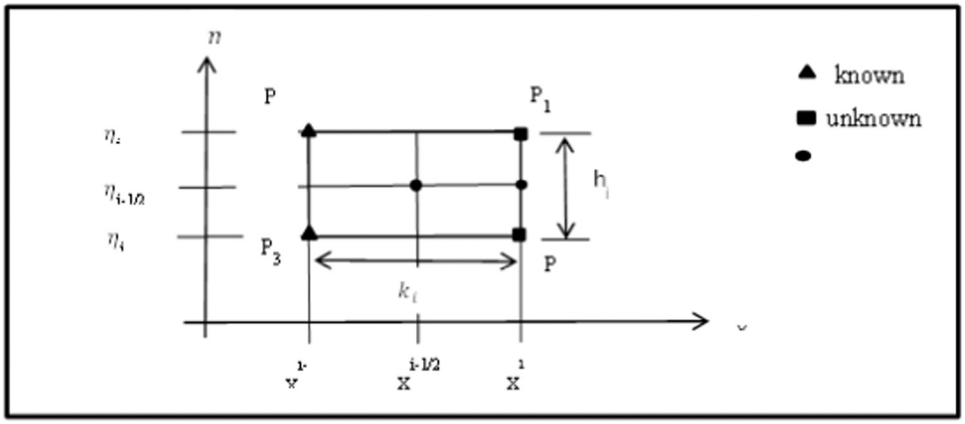

Fig. 1c. Net rectangle for finite difference approximations.

- The aspect of solar radiation is further considered for energy applications. Even in the absence of Soret and Dufour (SD) effects, this kind of research has not been done before.
- Here, it is preferred to take into account both mass transfer and heat transfer mechanisms using Soret and Dufour effects.
- Using Keller box approach, the governing nonlinear system solutions are calculated.

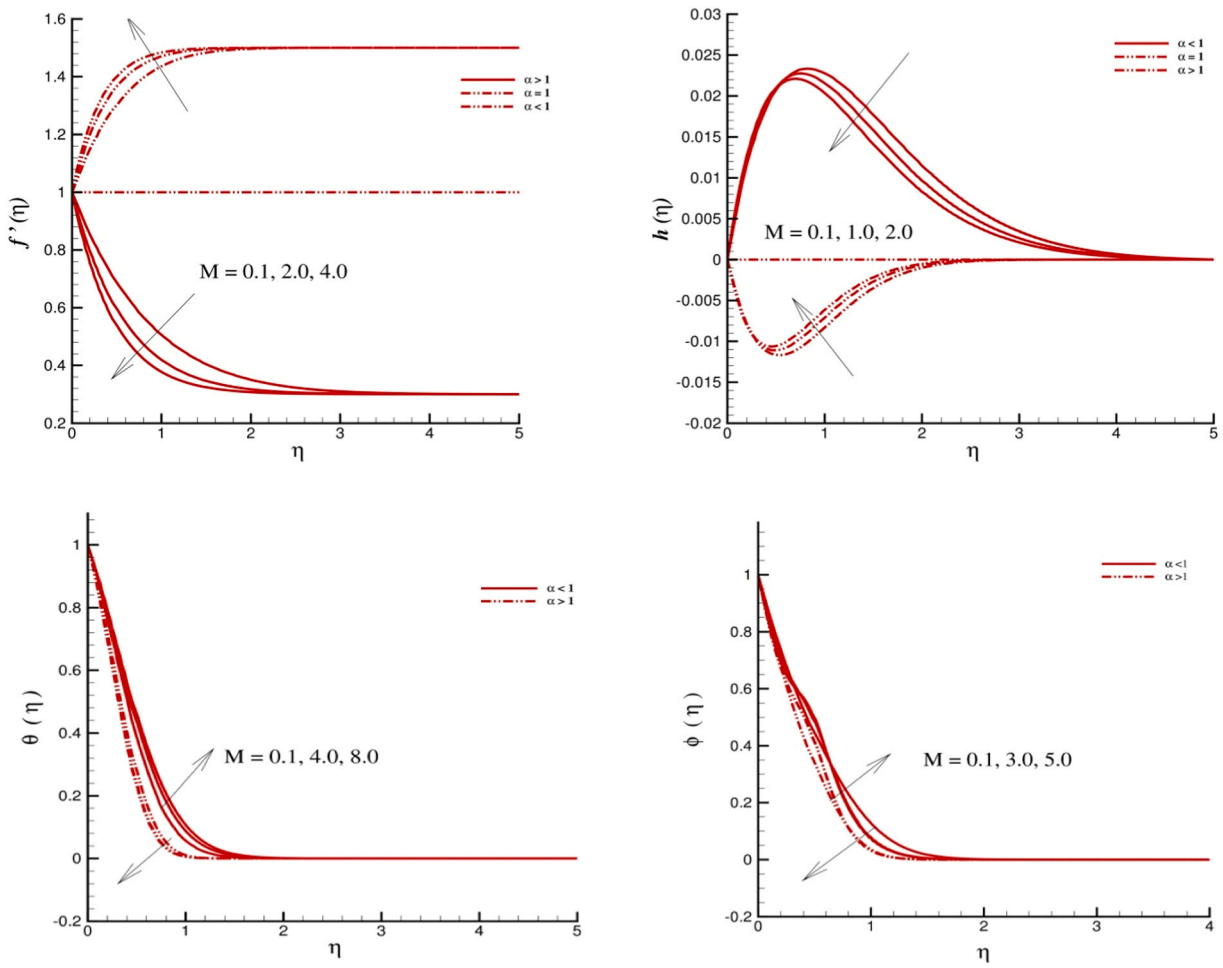

Fig. 2. Impacts of M on $f'(\eta)$, $h(\eta)$, $\theta(\eta)$ and $\phi(\eta)$.

- Comparative analysis is provided to validate our outcomes with existing one.
- In addition, a tabulated analysis is conducted on the impacts of different emerging parameters on the local Sherwood and Nusselt numbers and skin friction.

2. Problem formulation

We examine the Micropolar nanofluid flow over exponentially stretching surface. The flow is 2D and laminar. In thermal energy expression, the impacts of Soret and Dufour are considered. Solar radiation is accounted for further deep analysis of thermal field and for more realistic applications. Stagnation point flow is also considered. The Cartesian coordinates are considered for the flow analysis. Here, the stretched and free (ambient) stream velocities are considered as $u_w(x) = ae^{x/l}$ and $u \to u_\infty(x) = be^{x/l}$ where a and b both are constants and x is the axis computed along. the stretching sheet. Along with nanoparticles, the base fluid also contains rotating Micropolar finite sized particles. At the wall, T and C remain constant and are denoted by the T_w and C_w, where T stands for temperature and C for the concentration. Furthermore, the ambient values of T and C when y goes to infinity are T_∞ and C_∞ [57,58].

$$\frac{\partial u}{\partial x} + \frac{\partial v}{\partial y} = 0, \tag{1}$$

$$u\frac{\partial u}{\partial x} + v\frac{\partial u}{\partial y} = u_\infty \frac{du_\infty}{dx} - \frac{\sigma B^2}{\rho}(u - u_\infty) + \left(\frac{\mu}{k_1^*} + 1\right)\left(\frac{\partial^2 u}{\partial y^2} + \frac{\partial N^*}{\partial x}\right)\left(\frac{k_1^*}{\rho}\right) + g[\beta_t(T - T_\infty) + \beta_c(C - C_\infty)]Cos\Omega, \tag{2}$$

$$u\frac{\partial N^*}{\partial x} + v\frac{\partial N^*}{\partial y} = \left(\frac{\gamma^* k_1^*}{j^* \rho}\right)\left[\frac{1}{k_1^*}\frac{\partial^2 N^*}{\partial y^2} - \left(\frac{1}{\gamma^*}\right)\left(2N^* + \frac{\partial u}{\partial y}\right)\right], \tag{3}$$

$$u\frac{\partial T}{\partial x} + v\frac{\partial T}{\partial y} = \frac{1}{(\rho c)_f}\left(k\frac{\partial^2 T}{\partial y^2} - \frac{\partial q_r}{\partial y}\right) + \tau\left[D_B\frac{\partial C}{\partial y}\frac{\partial T}{\partial y} + \frac{D_T}{T_\infty}\left(\frac{\partial T}{\partial y}\right)^2\right] + \frac{D_T K_T}{c_s c_p}\frac{\partial^2 C}{\partial y^2}, \tag{4}$$

$$u\frac{\partial C}{\partial x} + v\frac{\partial C}{\partial y} = D_B\frac{\partial^2 C}{\partial y^2} + \frac{D_T K_T}{T_\infty}\frac{\partial^2 T}{\partial y^2} + \frac{D_B}{T_\infty}\left(\frac{\partial^2 C}{\partial y^2}\right). \tag{5}$$

The Rosseland approximation however, can be used to simplify the Eq. (4), which reduces the radiative heat flux to:

$$q_r = \frac{-4\sigma^*}{3k^*}\frac{\partial T^4}{\partial y}, \tag{6}$$

Where, respectively, σ* and k* stand for the Stefan-Boltzmann constant and the mean absorption coefficient. Without considering higher order terms, extending about T_∞, T_4 in a Taylor series results in:

$$T^4 = 4T_\infty^3 T - 3T_\infty^4, \tag{7}$$

Thus, simplified form of Eq. (4) is

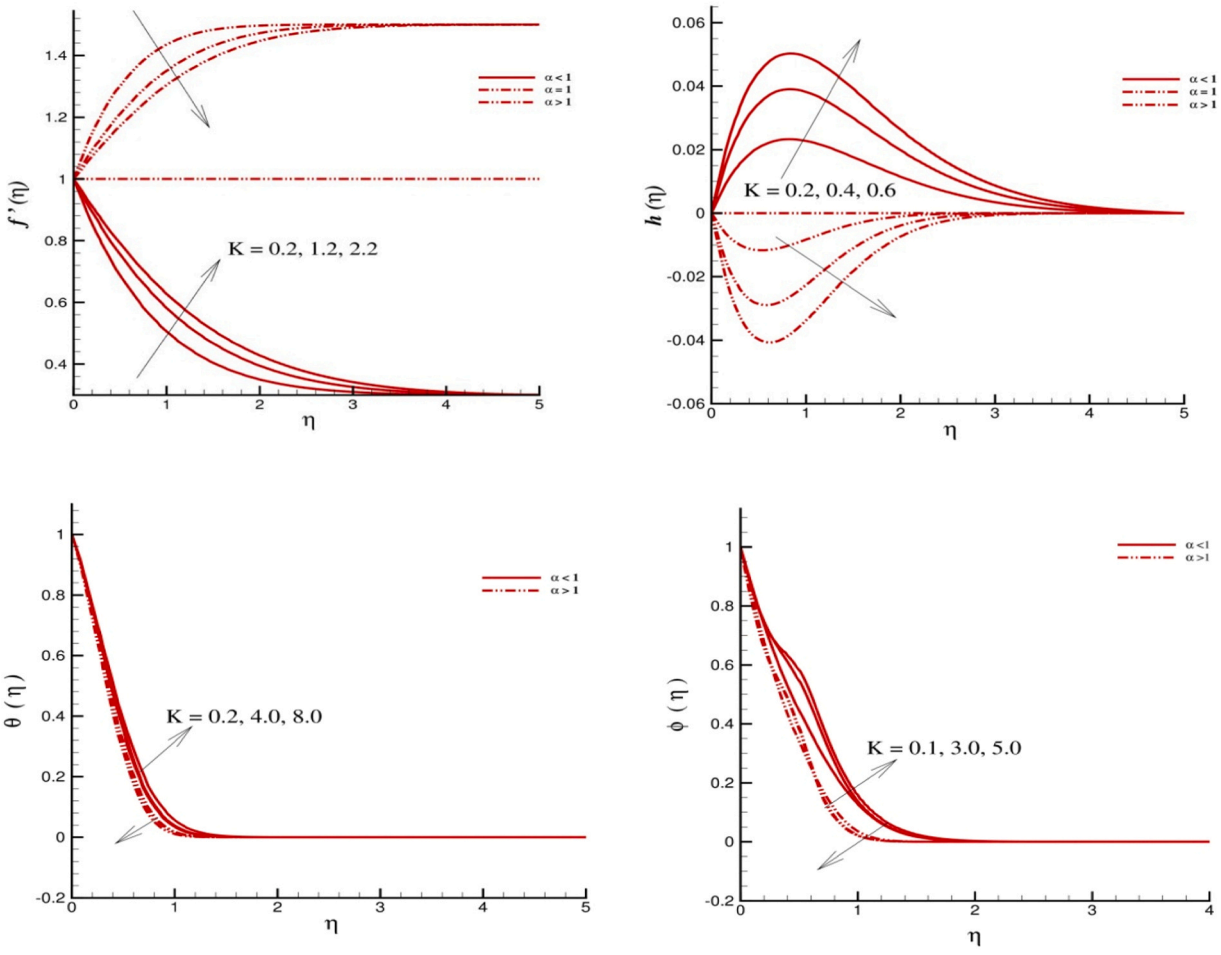

Fig. 3. Impacts of K on $f'(\eta)$, $h(\eta)$, $\theta(\eta)$ and $\phi(\eta)$.

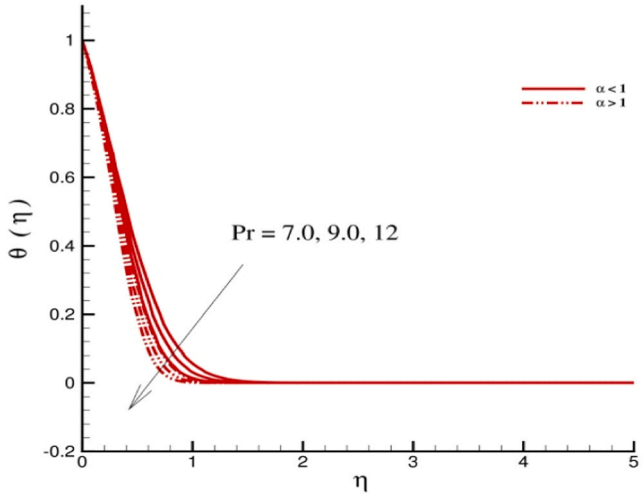

Fig. 4. Impacts Pr on (η).

$$u\frac{\partial T}{\partial x}+v\frac{\partial T}{\partial y}=\left(\alpha+\frac{16\sigma^{*}T_{\infty}^{3}}{3k^{*}(\rho c)_{f}}\right)\frac{\partial^{2}T}{\partial y^{2}}+\tau\left[D_{B}\frac{\partial C}{\partial y}\frac{\partial T}{\partial y}+\frac{D_{T}}{T_{\infty}}\left(\frac{\partial T}{\partial y}\right)^{2}\right], \tag{8}$$

Here u and v both are the respective velocity components i x and y directions, σ depicts the electrical conductivity, ρ represents base fluid's density, μ denotes viscosity, γ^{*} shows spin gradient viscosity, k_1^{*} depicts vertex viscosity, j^{*} denotes micro- inertia per unit mass, the thermal diffusivity parameter is $\alpha=\frac{k}{(\rho c)_f}$ where, $(\rho c)_f$, symbolizes base fluid heat capacity of base fluid and k is. known as thermal conductivity, Rd represents radiation parameter, $\tau=\frac{(\rho c)_p}{(\rho c)_f}$ is the relation between heat

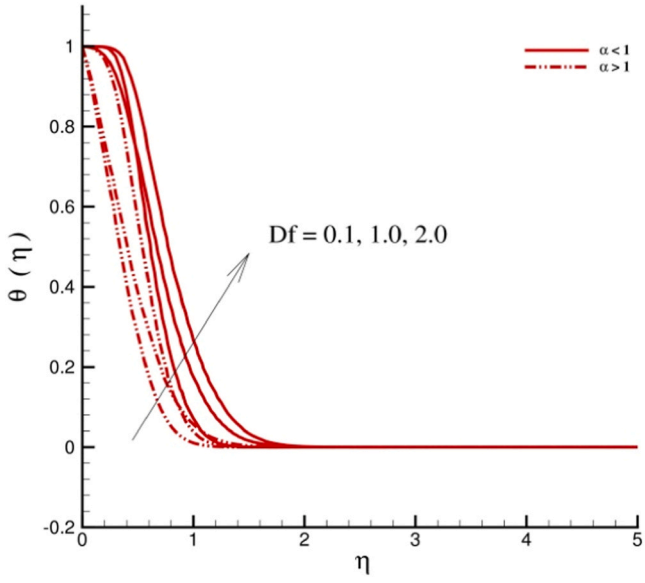

Fig. 5. Impacts D_f on $\theta(\eta)$.

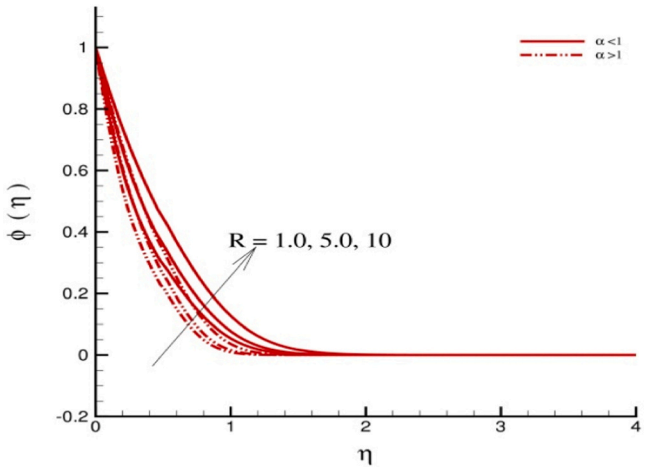

Fig. 6. Impacts R on $\phi(\eta)$.

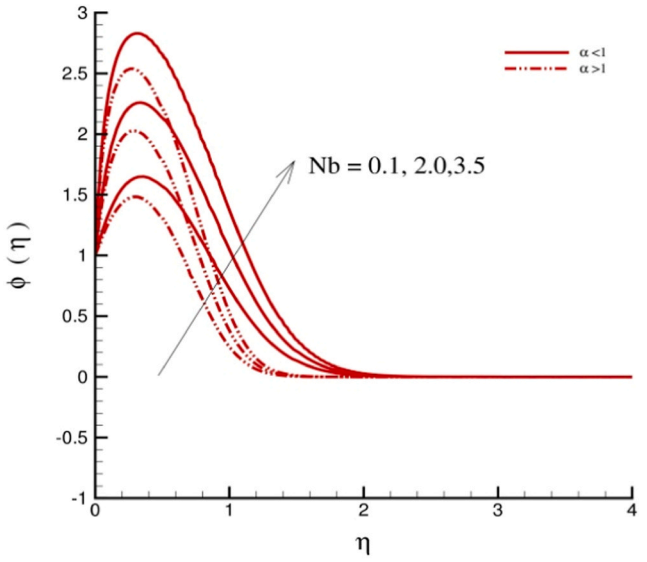

Fig. 7. Impacts Nb on $\phi(\eta)$.

capacity of nanoparticles and of liquids, furthermore, D_T stands for thermophoresis diffusion coefficient and D_B stands for Brownian motion, c_p depicts the specific heat and c_s represents the concentration susceptibility and the thermal diffusion ratio is depicted by K_T.

Boundary conditions that are imposed are listed below.

$$u = u_w(x) = ae^{x/l}, \quad v = 0, \quad N^* = -n_0\frac{\partial u}{\partial y}, \quad T = T_w(x), \quad C = C_w(x) at (y = 0),$$

$$u \to u_\infty = be^{x/l}, \quad v \to 0, \quad N^* \to 0, \quad T \to T_w, \quad C \to C_w as y \to \infty. \tag{9}$$

When $n_0 = 0$, it is implied that $N^* = 0$ at the wall, which stands for concentrated outline flow and deny the rotation of micro-elements along the surface of wall. In order to transfer the nonlinear PDE's into nonlinear ODE's, similarity transformations are defined. The stream function $\psi = \psi(x, y)$ is defined as follows for this use:

$$u = \frac{\partial \psi}{\partial y}, \quad v = -\frac{\partial \psi}{\partial x}. \tag{10}$$

The exponentially stretching sheet velocity is used to define the similarity transformations as follows:

$$\psi = \sqrt{2l\nu a}\; e^{\frac{x}{2l}} f(\eta), N^* = \left(\frac{a}{2\nu l}\right) e^{\frac{3x}{2l}} \sqrt{2l\nu a} h(\eta), \theta(\eta) = \frac{T - T_\infty}{T_w - T_\infty}, \eta = ae^{\frac{x}{2l}} f'(\eta) y$$

$$\phi(\eta) = \frac{C - C_\infty}{C_w - C_\infty}.$$

Where,

$$T_w = T_\infty + T_0 e^{\frac{x}{2l}}, \qquad C_w = C_\infty + C_0 e^{\frac{x}{2l}}. \tag{11}$$

Equations (2, 3, 5 and 8) are converted to the following nonlinear ODE's when Eq. (11) is substituted:

$$(1 + K)f''' + ff'' - 2f'^2 + 2\alpha^2 + Kh' - M(f' - \alpha) + (\lambda\theta + \delta\phi)Cos\Omega = 0, \tag{12}$$

$$\left(1 + \frac{K}{2}\right)h'' + h'f - 3f'h - K(2h + f'') = 0, \tag{13}$$

$$\left(1 + \frac{4}{3}Rd\right)\frac{1}{\Pr}\theta'' + \theta' f - \theta f' + \theta'(Nb\phi' + Nt\theta') + D_f\phi'' = 0, \tag{14}$$

$$\phi'' - Sc(\phi f' - \phi' f + S_r\theta'' + \frac{Nt}{Nb}\theta'') = 0; \tag{15}$$

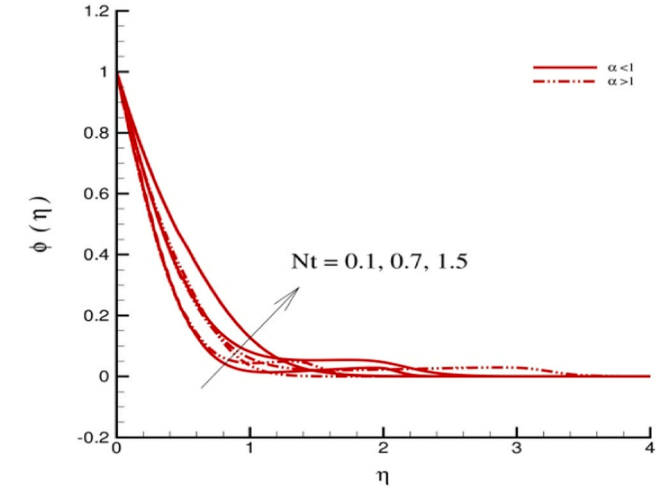

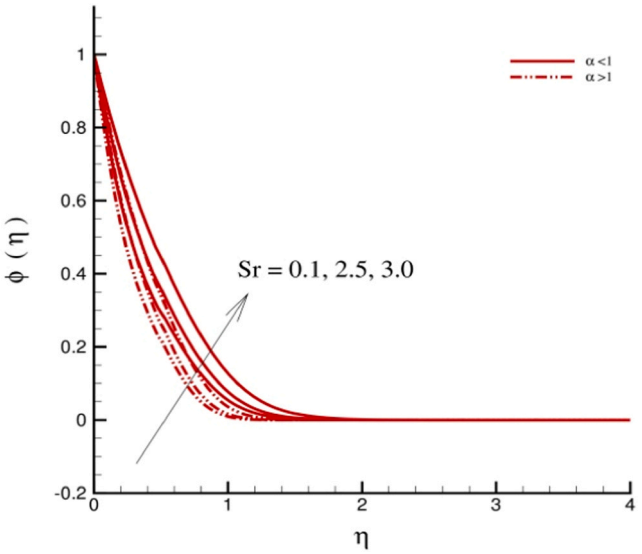

Fig. 8. (a). Impacts Nt on $\phi(\eta)$. (b). Impacts Sr on $\phi(\eta)$.,.

Here, prime denotes derivatives with respect to η, $M = \frac{2I\sigma B^2}{a\rho}$ represents magnetic parameter are known as the Hartmann number, the Prandtl number is depicted by $\Pr = \frac{\nu}{\alpha}$, $K = \frac{k_1^*}{\mu}$ depicts dimensionless vortex viscosity, $\alpha = \frac{b}{a}$ velocity ratio parameter, $Rd = \frac{4\sigma^* T_\infty^3}{kk^*}$ radiation parameter, ν is fluid's kinematic viscosity, the Schmidt number is. $Sc = LePr = \frac{\nu}{D_B}$, $Nt = \frac{\tau D_T (T_w - T_\infty)}{\nu T_\infty}$.is thermophoresis parameter and $Nb = \frac{D_B \tau (C_w - C_\infty)}{\nu}$ is Brownian motion parameter, $\lambda = \frac{G_r}{\mathrm{Re}_x^2}$ is buoyancy parameter, $G_r = \frac{2gB_t(T_w - T_\infty)l^3}{\nu^2}$ is local Grashof number, $\delta = \frac{G_C}{\mathrm{Re}_x^2}$ is solutal buoyancy parameter and $G_c = \frac{2gB_c(C_w - C_\infty)l^3}{\nu^2}$ is local Grashof number, Soret number is represented by $S_r = \frac{D_T k_T (T_w - T_\infty)}{\nu T_\infty (C_w - C_\infty)}$ and Dufour number by $D_f = \frac{D_m k_T (C_w - C_\infty)}{\nu c_s c_p (T_w - T_\infty)}$.

The imposed conditions (9) are transformed to

$$f'(\eta) = 1, \quad f(\eta) = 0,\ h(\eta) = -n_0 f''(\eta), \phi(\eta) = 1, \theta(\eta) = 1, at\ \eta = 0,$$

$$f'(\eta) \to \gamma, \theta(\eta) \to 0,\ h(\eta) \to 0,\ \phi(\eta) \to 0\ as\ \eta \to \infty. \tag{16}$$

The Sherwood number (Sh), the skin friction (C_{fx}) and the Nusselt number (Nu) are as follows:

$$Sh = \frac{xq_m}{D_B(C_w - C_\infty)} \quad , Nu = \frac{xq_w}{k(T_w - T_\infty)} + q_r \quad , \quad C_{fx} = \frac{\tau_w}{\rho u_w^2}. \tag{17}$$

Where,

$$\tau_w = \left(\mu + k_1^*\right)\frac{\partial u}{\partial y} + k_1^* N^*, \quad q_w = -k\frac{\partial T}{\partial y} and q_m = -D_B\frac{\partial C}{\partial y} at y = 0 \tag{18}$$

are the respective shear stress and the heat and mass fluxes at the surface. In the view of Eq. (10), Eq. (17) becomes:

$$C_{fx}(0) = C_f\sqrt{\mathrm{Re}_x}, \quad -\phi'(0) = \frac{Sh}{\sqrt{\mathrm{Re}_x}}, \quad -\theta'(0) = \frac{Nu}{(1 + Rd\frac{4}{3})\sqrt{\mathrm{Re}_x}}. \tag{19}$$

Here,.the local Reynolds number is $\mathrm{Re}_x = \frac{axe^{x/l}}{\nu}$.

3. Keller Box method

3.1. The finite- difference method

Equations (12–15) with imposed boundary conditions (16) can be expressed in a system of the 1st order ODE's as:

$$(1+K)v' + fv - 2u^2 + Kl - M(u - \alpha) + 2\alpha^2 + (\lambda g + \delta q)Cos\Omega = 0,$$

$$\left(1 + \frac{K}{2}\right)l' + lf - 3ut - K(2t + v) = 0,$$

$$\left(1 + \frac{4Rd}{3}\right)\frac{1}{\Pr}p' + fp - ug + p(Nbs + Ntp) + D_f s' = 0,$$

$$s' - Sc(qu - fs + S_r p' + \frac{Nt}{Nb}p') = 0, \tag{20}$$

Where,

$$u(\eta) = f'(\eta), \quad v(\eta) = u'(\eta), p(\eta) = g'(\eta), \quad l(\eta) = t'(\eta), \quad s(\eta) = q'(\eta).$$

In terms of (η), the BC's can be written as:

$$u(\eta) = 1, f(\eta) = 0, \quad h(\eta) = -v(\eta)n_0, g(\eta) = 1, \quad q(\eta) = 1 at\ \eta = 0,$$

$$u(\eta) \to \gamma, \quad h(\eta) \to 0, g(\eta) \to 0, q(\eta) \to 0\ as\ \eta \to \infty. \tag{21}$$

In the $x - \eta$ plane the net rectangle is assumed and expressed as:

$$x^0 = 0, \qquad x^i = x^{i-1} + k_i, \quad i = 1, 2, 3, 4, \ldots, I,$$

$$\eta_0 = 0, \quad \eta_j = \eta_{j-1} + h_j, \quad j = 1, \quad 2, \quad 3, \quad 4, \ldots J, \quad \eta_J \equiv \eta_\infty. \tag{22}$$

Where, Δx spaces represented by k_i whereas, $\Delta\eta$ spaces represented by h_i. In this case, i and j are merely a series of integers which represents the position of coordinates and are not tensor indices exponents.

With Finite Differences, the derivatives in x and η directions provided as:

$$\frac{\partial u}{\partial x} = \frac{u^i - u^{i-1}}{k_i}, \quad \frac{\partial v}{\partial \eta} = v' = \frac{v_j - v_{j-1}}{h_j}, \tag{23}$$

In general case, for some points

$$\frac{\left[()_j^i + ()_j^{i-1}\right]}{2} = ()_j^{i-1/2}, \text{and} \frac{[()_j^i + ()_{j-1}^i]}{2} = ()_{j-1/2}^i. \tag{24}$$

The difference equations "centring about $(\eta_{j-1/2})$" to app. (20) are given below.

$$u_{j-1/2}^i = \frac{\left(u_j^i + u_{j-1}^i\right)}{2} = \frac{\left(\ f_j^i - f_{j-1}^i\right)}{h_j},$$

$$l_{j-1/2}^i = \frac{\left(l_j^i + l_{j-1}^i\right)}{2} = \frac{(t_j^i - t_{j-1}^i)}{h_j},$$

$$s_{j-1/2}^i = \frac{\left(s_j^i + s_{j-1}^i\right)}{2} = \frac{(q_j^i - q_{j-1}^i)}{h_j},$$

$$v_{j-1/2}^i = \frac{\left(v_j^i + v_{j-1}^i\right)}{2} = \frac{(u_j^i - u_{j-1}^i)}{h_j},$$

$$p_{j-1/2}^i = \frac{\left(p_j^i + p_{j-1}^i\right)}{2} = \frac{(g_j^i - g_{j-1}^i)}{h_j}. \tag{25}$$

$$(1+K)\left(\frac{v_j - v_{j-1}}{h_j}\right) + \left[\left(\frac{f_j + f_{j-1}}{2}\right)\left(\frac{v_j + v_{j-1}}{2}\right)\right] - 2\left[\left(\frac{u_j + u_{j-1}}{2}\right)^2\right] + K\left(\frac{l_j + l_{j-1}}{2}\right) + M\left[\alpha - \left(\frac{u_j + u_{j-1}}{2}\right)\right] + 2\alpha^2 + \lambda\cos\Omega\left(\frac{g_j + g_{j-1}}{2}\right) + \delta\cos\Omega\left(\frac{q_j + q_{j-1}}{2}\right) = 0,$$

$$\left(1 + \frac{K}{2}\right)\left(\frac{l_j - l_{j-1}}{h_j}\right) + \left[\left(\frac{l_j + l_{j-1}}{2}\right)\left(\frac{f_j + f_{j-1}}{2}\right)\right] - 3\left[\left(\frac{u_j + u_{j-1}}{2}\right)\left(\frac{t_j + t_{j-1}}{2}\right)\right] - K\left[2\left(\frac{t_j + t_{j-1}}{2}\right) + \left(\frac{v_j + v_{j-1}}{2}\right)\right] = 0,$$

$$\frac{1}{\Pr}\left(1 + \frac{4Rd}{3}\right)\left(\frac{p_j - p_{j-1}}{h_j}\right) + \left[\left(\frac{f_j + f_{j-1}}{2}\right)\left(\frac{p_j + p_{j-1}}{2}\right)\right] - \left[\left(\frac{u_j + u_{j-1}}{2}\right)\left(\frac{g_j + g_{j-1}}{2}\right)\right] + Nb\left[\left(\frac{p_j + p_{j-1}}{2}\right)\left(\frac{s_j + s_{j-1}}{2}\right)\right] + Nt\left(\frac{p_j + p_{j-1}}{2}\right)^2 + D_f\left(\frac{s_j - s_{j-1}}{h_j}\right) = 0,$$

$$\left(\frac{s_j - s_{j-1}}{h_j}\right) + Sc\{\left[\left(\frac{f_j + f_{j-1}}{2}\right)\left(\frac{s_j + s_{j-1}}{2}\right)\right] - \left[\left(\frac{q_j + q_{j-1}}{2}\right)\left(\frac{u_j + u_{j-1}}{2}\right)\right] + S_r\left(\frac{p_j - p_{j-1}}{h_j}\right) + Le\frac{Nt}{Nb}\left(\frac{p_j - p_{j-1}}{h_j}\right)\} = 0. \quad (26)$$

η transforms, the boundary conditions (21) at $x = x_i$ into

$$f_0^i = 0, \quad u_0^i = 1, \quad h_0^i = -n_0 v_0^i, \quad g_0^i = 1, \quad q_0^i = 1,$$

$$u_J^i = \varepsilon, \quad h_J^i = 0, \quad g_J^i = 0, \quad q_J^i = 0. \quad (27)$$

3.2. The Newton's Method

If $\left(f_j^{i-1}, \ u_j^{i-1}, \ v_j^{i-1}, \ t_j^{i-1}, \ l_j^{i-1}, \ g_j^{i-1}, \ p_j^{i-1}, \ qands_j^{i-1}\right)$ are known values for $0 \le j \le J$. Then, the solution has to be find out for the unknowns $\left(f_j^i, \ u_j^i, \ v_j^i, \ t_j^i, \ l_j^i, \ g_j^i, \ p_j^i, \ q_j^i and s_j^i\right), \quad 0 \le j \le J$. For simplicity, after removing the quadratic and higher order expressions along the superscript i as $(\delta f_j^{(k)}, \delta u_j^{(k)}, \delta v_j^{(k)}, \delta t_j^{(k)}, \delta l_j^{(k)}, \delta g_j^{(k)}, \delta p_j^{(k)}, \delta q_j^{(k)}, and \ \delta s_j^{(k)})$.

$$(r_1)_{j-1/2} = \left(\delta f_j - \delta f_{j-1}\right) - \frac{h_j\left(\delta u_j - \delta u_{j-1}\right)}{2}$$

$$(r_2)_{j-1/2} = \left(\delta u_j - \delta u_{j-1}\right) - \frac{h_j\left(\delta v_j - \delta v_{j-1}\right)}{2}$$

$$(r_3)_{j-1/2} = \left(\delta t_j - \delta t_{j-1}\right) - \frac{h_j\left(\delta l_j - \delta l_{j-1}\right)}{2}$$

$$(r_4)_{j-1/2} = \left(\delta g_j - \delta g_{j-1}\right) - \frac{h_j\left(\delta p_j - \delta p_{j-1}\right)}{2}$$

$$(r_5)_{j-1/2} = \left(\delta q_j - \delta q_{j-1}\right) - \frac{h_j\left(\delta s_j - \delta s_{j-1}\right)}{2}$$

$$\begin{aligned}(r_6)_{j-1/2} = {} & (a_1)_j\delta v_j + (a_2)_j\delta v_{j-1} + (a_3)_j\delta f_j + (a_4)_j\delta f_{j-1} + (a_5)_j\delta u_j \\ & + (a_6)_j\delta u_{j-1} + (a_7)_j\delta l_j + (a_8)_j\delta l_{j-1} + (a_9)_j\delta g_j + (a_{10})_j\delta g_{j-1} \\ & + (a_{11})_j\delta q_j + (a_{12})_j\delta q_{j-1}\end{aligned}$$

$$\begin{aligned}(r_7)_{j-1/2} = {} & \delta l_j(b_1)_j + \delta l_{j-1}(b_2)_j + \delta f_j(b_3)_j + \delta f_{j-1}(b_4)_j + (b_5)_j\delta u_j + \delta u_{j-1}(b_6)_j \\ & + \delta v_j(b_7)_j + \delta v_{j-1}(b_8)_j + \delta t_j(b_9)_j + \delta t_{j-1}(b_{10})_j\end{aligned}$$

$$\begin{aligned}(r_8)_{j-1/2} = {} & (c_1)_j\delta p_j + (c_2)_j\delta p_{j-1} + (c_3)_j\delta f_j + (c_4)_j\delta f_{j-1} + (c_5)_j\delta u_j \\ & + (c_6)_j\delta u_{j-1} + (c_7)_j\delta g_j + (c_8)_j\delta g_{j-1} + (c_9)_j\delta s_j + (c_{10})_j\delta s_{j-1}\end{aligned}$$

$$\begin{aligned}(r_9)_{j-1/2} = {} & (d_1)_j\delta s_j + (d_2)_j\delta s_{j-1} + (d_3)_j\delta f_j + (d_4)_j\delta f_{j-1} + (d_5)_j\delta u_j \\ & + (d_6)_j\delta u_{j-1} + (d_7)_j\delta q_j + (d_8)_j\delta q_{j-1} + (d_9)_j\delta p_j + (d_{10})_j\delta p_{j-1}.\end{aligned}$$

Where,

$(a_1)_j = K + 1 + f_{j-1/2}, \ (a_2)_j = -(1+K) + \frac{h_j}{2}f_{j-1/2}, \ (a_3)_j = \frac{h_j}{2}v_{j-1/2}, \ (a_4)_j = (a_3)_j, \ (a_5)_j = -\frac{h_j}{2}M - h_j u_{j-1/2}, \ (a_6)_j = (a_5)_j, \ (a_7)_j = K\frac{h_j}{2}, \ (a_8)_j = (a_7)_j, \ (a_9)_j = \frac{h_j}{2}\lambda\cos\Omega, \ (a_{10})_j = (a_9)_j, \ (a_{11})_j = \frac{h_j}{2}\delta\cos\Omega, \ (a_{12})_j = (a_{11})_j.$

$(b_1)_j = (1 + \frac{K}{2}) + \frac{h_j}{2}f_{j-1/2}, (b_2)_j = -\left(1 + \frac{K}{2}\right) + \frac{h_j}{2}f_{j-1/2}, \ (b_3)_j = \frac{h_j}{2}l_{j-1/2}, \ (b_4)_j = (b_3)_j, \ (b_5)_j = -3\frac{h_j}{2}t_{j-1/2}, \ (b_6)_j = (b_5)_j, (b_7)_j = -K\frac{h_j}{2}, \ (b_8)_j = (b_7)_j, \ (b_9)_j = -3\frac{h_j}{2}u_{j-1/2} - Kh_j, \ (b_{10})_j = (b_9)_j.$

$$\begin{aligned}(c_1)_j = {} & \left(1 + \frac{4Rd}{3}\right) + PrNb\frac{h_j}{2}s_{j-1/2} + NtPr\frac{h_j}{2}p_{j-1/2} - \Pr\frac{h_j}{2}f_{j-1/2}, \\ (c_2)_j = {} & -\left(1 + \tfrac{4Rd}{3}\right) + PrNb\tfrac{h_j}{2}s_{j-1/2} + NtPr\tfrac{h_j}{2}p_{j-1/2} - \Pr\tfrac{h_j}{2}f_{j-1/2}, (c_3)_j = \\ & \Pr\tfrac{h_j}{2}p_{j-1/2}, \quad (c_4)_j = (c_3)_j \quad (c_5)_j = \Pr\tfrac{h_j}{2}g_{j-1/2}, \quad (c_6)_j = (c_5)_j \quad (c_7)_j = - \\ & \Pr\tfrac{h_j}{2}u_{j-1/2}, (c_8)_j = (c_7)_j \ , \ (c_9)_j = NbPr\tfrac{h_j}{2}p_{j-1/2} + D_f\Pr, (c_{10})_j = (c_9)_j,\end{aligned}$$

$$\begin{aligned}& (d_1)_j = 1 + Sc\frac{h_j}{2}f_{j-1/2}, (d_2)_j = -1 + Sc\frac{h_j}{2}f_{j-1/2}, \ (d_3)_j = Sc\frac{h_j}{2}s_{j-1/2}, \\ & (d_4)_j = (d_3)_j, (d_5)_j = -Sc\frac{h_j}{2}q_{j-1/2}, \ (d_6)_j = (d_5)_j, (d_7)_j = -Sc\frac{h_j}{2}u_{j-1/2} \ , \\ & (d_8)_j = (d_7)_j, \ (d_9)_j = -ScS_r - Sc\frac{Nr}{Nb}, (d_{10})_j = ScS_r + Le\frac{Nr}{Nb}. \quad (28)\end{aligned}$$

And

$$(r_1)_{j-1/2} = f_{j-1} - f_j + h_j u_{j-1/2},$$

$$(r_2)_{j-1/2} = u_{j-1} - u_j + h_j v_{j-1/2},$$

$$(r_3)_{j-1/2} = t_{j-1} - t_j + h_j l_{j-1/2},$$

$$(r_4)_{j-1/2} = g_{j-1} - g_j + h_j p_{j-1/2},$$

$$(r_5)_{j-1/2} = q_{j-1} - q_j + h_j s_{j-1/2},$$

$$\begin{aligned}(r_6)_{j-1/2} = {} & (1+K)(v_{j-1} - v_j) - h_j f_{j-1/2}v_{j-1/2} + 2h_j u_{j-1/2}^2 - h_j K l_{j-1/2} \\ & - M\alpha h_j + h_j M u_{j-1/2} - 2\alpha^2 h_j - \lambda\cos\Omega h_j g_{j-1/2} - \delta\cos\Omega h_j q_{j-1/2},\end{aligned}$$

$$(r_7)_{j-1/2} = \left(1 + \frac{K}{2}\right)(l_{j-1} - l_j) - h_j f_{j-1/2}l_{j-1/2} + 3h_j u_{j-1/2}t_{j-1/2} + h_j 2Kt_{j-1/2}$$

$$+ h_j K v_{j-1/2},$$

$$(r_8)_{j-1/2} = \left(1 + \frac{4Rd}{3}\right)\left(p_{j-1} - p_j\right) - h_j Prf_{j-1/2}p_{j-1/2} + Prh_j u_{j-1/2}g_{j-1/2}$$

$$-PrNbh_j s_{j-1/2}p_{j-1/2} - NtPrh_j p_{j-1/2}^2 - D_f\Pr(s_j - s_{j-1}),$$

$$(r_9)_{j-1/2} = (s_{j-1} - s_j) - Sch_j f_{j-1/2}s_{j-1/2} - Sch_j q_{j-1/2}u_{j-1/2} + ScS_r(p_{j-1} - p_j)$$

$$+ Sc\frac{Nt}{Nb}(p_{j-1} - p_j). \quad (29)$$

The boundary conditions (26) are

$$\delta f_0 = 0, \delta h_0 = 0, \delta q_0 = 0, \delta u_0 = 0, \delta g_0 = 0 \quad ,$$

$$\delta u_J = 0, \delta g_J = 0, \delta h_J = 0, \delta q_J = 0. \quad (30)$$

3.3. The block-elimination method

The block tri-diagonal structure frequently consists of constants or variables, but a noteworthy characteristic of the Keller-box method is that it also incorporates block matrices when considering. $l = -\frac{h_j}{2}$, and defined as

$$[A_1]=\begin{bmatrix} 0 & 0 & 0 & 0 & 1 & 0 & 0 & 0 & 0\\ l & 0 & 0 & 0 & 0 & l & 0 & 0 & 0\\ 0 & l & 0 & 0 & 0 & 0 & l & 0 & 0\\ 0 & 0 & l & 0 & 0 & 0 & 0 & l & 0\\ 0 & 0 & 0 & l & 0 & 0 & 0 & 0 & l\\ (a_2)_1 & (a_8)_1 & 0 & 0 & (a_3)_1 & (a_1)_1 & (a_7)_1 & 0 & 0\\ (b_8)_1 & (b_2)_1 & 0 & 0 & (b_3)_1 & (b_7)_1 & (b_1)_1 & 0 & 0\\ 0 & 0 & (c_2)_1 & (c_{10})_1 & (c_3)_1 & 0 & 0 & (c_1)_1 & (c_9)_1\\ 0 & 0 & (d_{10})_1 & (d_2)_1 & (d_3)_1 & 0 & 0 & (d_9)_1 & (d_1)_1 \end{bmatrix}$$

$$[A_j]=\begin{bmatrix} l & 0 & 0 & 0 & 1 & 0 & 0 & 0 & 0\\ -1 & 0 & 0 & 0 & 0 & l & 0 & 0 & 0\\ 0 & -1 & 0 & 0 & 0 & 0 & l & 0 & 0\\ 0 & 0 & -1 & 0 & 0 & 0 & 0 & l & 0\\ 0 & 0 & 0 & -1 & 0 & 0 & 0 & 0 & l\\ (a_6)_j & 0 & (a_{10})_j & (a_{12})_j & (a_3)_j & (a_1)_j & (a_7)_j & 0 & 0\\ (b_6)_j & (b_{10})_j & 0 & 0 & (b_3)_j & (b_7)_j & (b_1)_j & 0 & 0\\ (c_6)_j & 0 & (c_8)_j & 0 & (c_3)_j & 0 & 0 & (c_1)_1 & (c_9)_j\\ (d_6)_j & 0 & 0 & (d_8)_j & (d_3)_j & 0 & 0 & (d_9)_1 & (d_1)_j \end{bmatrix}, \quad 2\le j \le J,$$

$$[B_j]=\begin{bmatrix} 0 & 0 & 0 & 0 & -1 & 0 & 0 & 0 & 0\\ 0 & 0 & 0 & 0 & 0 & l & 0 & 0 & 0\\ 0 & 0 & 0 & 0 & 0 & 0 & l & 0 & 0\\ 0 & 0 & 0 & 0 & 0 & 0 & 0 & l & 0\\ 0 & 0 & 0 & 0 & 0 & 0 & 0 & 0 & l\\ 0 & 0 & 0 & 0 & (a_4)_j & (a_2)_j & (a_8)_j & 0 & 0\\ 0 & 0 & 0 & 0 & (b_4)_j & (b_8)_j & (b_2)_j & 0 & 0\\ 0 & 0 & 0 & 0 & (c_4)_j & 0 & 0 & (c_2)_j & (c_{10})_j\\ 0 & 0 & 0 & 0 & (d_4)_j & 0 & 0 & (d_{10})_j & (d_2)_j \end{bmatrix}, \quad 2\le j \le J,$$

$$[C_j]=\begin{bmatrix} l & 0 & 0 & 0 & 0 & 0 & 0 & 0 & 0\\ 1 & 0 & 0 & 0 & 0 & 0 & 0 & 0 & 0\\ 0 & 1 & 0 & 0 & 0 & 0 & 0 & 0 & 0\\ 0 & 0 & 1 & 0 & 0 & 0 & 0 & 0 & 0\\ 0 & 0 & 0 & 1 & 0 & 0 & 0 & 0 & 0\\ (a_5)_j & 0 & (a_9)_j & (a_{11})_j & 0 & 0 & 0 & 0 & 0\\ (b_5)_j & (b_9)_j & 0 & 0 & 0 & 0 & 0 & 0 & 0\\ (c_5)_j & 0 & (c_7)_j & 0 & 0 & 0 & 0 & 0 & 0\\ (d_5)_j & 0 & 0 & (d_7)_j & 0 & 0 & 0 & 0 & 0 \end{bmatrix}, \quad 1\le j \le J-1,$$

$$[\delta_1]=\begin{bmatrix} \delta v_0\\ \delta l_0\\ \delta p_0\\ \delta s_0\\ \delta f_1\\ \delta v_1\\ \delta l_1\\ \delta p_1\\ \delta s_1 \end{bmatrix}, [\delta_j]=\begin{bmatrix} \delta u_{j-1}\\ \delta t_{j-1}\\ \delta g_{j-1}\\ \delta q_{j-1}\\ \delta f_j\\ \delta v_j\\ \delta l_j\\ \delta p_j\\ \delta s_j \end{bmatrix}, 2\le j\le J, [r_j]=\begin{bmatrix} (r_1)_{j-1/2}\\ (r_2)_{j-1/2}\\ (r_3)_{j-1/2}\\ (r_4)_{j-1/2}\\ (r_5)_{j-1/2}\\ (r_6)_{j-1/2}\\ (r_7)_{j-1/2}\\ (r_8)_{j-1/2}\\ (r_9)_{j-1/2} \end{bmatrix}, 1\le j\le J.$$

4. Discussion and outcomes

The Keller box technique is employed to execute the nonlinear ODE's (12–15) that are subjected to BC's (16). The results for the relevant physical parameters, such as $Nb, Pr, M, Rd, \delta, \Omega, Nt, Le, K, \lambda$, and α are presented in tabular form by using Table 1 and 2. When δ, Nt, K, α, Nb, λ, and Le are equal to zero and $\Omega = 90^0$. Table 1 depicts the comparison of current findings for $-\theta'(0)$ to the findings from Bidin and Nazar [57] and Ishak [58]. Here, a good consensus can be seen in this comparison.

The ranges of different parameters are selected as $0.1 \le K \le 8,\ 0.1 \le Nb \le 3,\ 0.5 \le Nt \le 3,\ 0.1 \le M \le 8,\ 5 \le Sc \le 10,\ 0.1 \le D_f \le 2,\ 0.1 \le Sr \le 3,\ 6.2 \le \Pr \le 12,\ 0.1 \le Rd \le 10$. To illustrate how $\theta'(0)$, $\phi'(0)$, and $C_{fx}(0)$ vary for various values of Le, Pr, M, Nb, δ, Ω, Nt, Rd, S_r, D_f, K, λ and γ, Table 2 is constructed. It has been found that when $K, S_r, D_f, \lambda, \delta$ and α are higher, $\theta'(0)$ grows, whereas it decays for increasing Nb, Nt, Pr, M and Ω. For increasing.values of Le and Rd, . the local reduced Nusselt number gives negative values. The table 2, however, clearly demonstrates that $-\phi'(0)$ is decreasing while rising, β, S_r and M. While, rising with higher values of $Nb, Nt, Pr, Sc, K, Rd, \lambda, \delta$ and α. Additionally, it has been discovered that $C_{fx}(0)$ decreases as $Nb, Nt, Rd, S_r, \alpha, \delta$ and λ grows and increases when $\Pr, Sc, \Omega, K, M$ and D_f values rise.

Effects of magnetic variable on velocity, angular velocity, temperature and concentration profile for $\alpha < 1$ and $\alpha > 1$ are presented in Fig. 2. It is clear that velocity, angular velocity profile and concentration profile gives similar behavior, but temperature profile moves in an opposite manner. It indicates that if the magnetic field intensity is uplifted, $f'(\eta)$ and $h(\eta)$ decreases for $\alpha < 1$ and grows for $\alpha > 1$. Therefore an enhancement in M significantly decays the nanofluid velocity. Physically, a resistive force is generated by employing the magnet to the flow, which greatly resists the nanomaterils velocity. It is discovered that when the magnetic field is stronger, the nanoliquid's velocity decreases for $\alpha > 1$. This feature can be explained physically by the fact that Lorentz force increases with increasing magnetic parameters, creating significant resistance to fluid motion. In the end, the collision of the nanoparticles intensifies and the corresponding momentum boundary layer falls. Features of vortex viscosity on angular velocity, velocity, temperature and concentration profiles for $\alpha < 1$ and $\alpha > 1$ are represented by Fig. 3. It indicates that when the vortex viscosity is increased, $f'(\eta)$, $h(\eta)$ and $\theta(\eta)$ increases for $\alpha < 1$ and decreases for $\alpha > 1$ but $\theta(\eta)$ shows a decreasing behavior for $\alpha < 1$ $(i.e\alpha = 0.3)$ and increasing behavior for $\alpha > 1$ $(i.e\alpha = 1.3)$.

Impacts Pr on temperature is shown in Fig. 4. It is observed that increased Prandtl number, the thermal field of the nanoliquid declines. As Pr rises, the thermal diffusivity decreases as a result of the rapid heat transfer that lowers the temperature distribution. Fig. 5 illustrates how the temperature profile grew for both cases i.e. $\alpha < 1$ and $\alpha > 1$, when the parameter D_f reached higher values. It makes sense because a rise in the D_f led to an increase in gradient of concentration, which accelerated mass diffusion. The rate of energy transfer associated with the particles increased in this way. The temperature profile was improved for this reason. Fig. 6 shows how the temperature profile behaves when compared to the radiation Rd. Nanomaterials temperature rises as the Rd improves; as a result, heat is produced in the flow field, which raises the. temperature. See Figs. 7 and 8(a) for the effects of Nt and Nb on concentration profile. The relationship between the concentration outline and above mentioned parameters is direct for both cases for $\alpha < 1$ $(i.e\alpha = 0.3)$ and for $\alpha > 1$ $(i.e\alpha = 1.3)$. The concentration profile directly varies in relation to the Soret factor depicted in Fig. 8(b).

5. Conclusions

The investigation of' the stagnation point flow of a Micropolar nanofluid toward an inclined exponential stretchable surface has been examined in this article. The impacts of the Soret and Dufour are also incorporated in the flow field. The main outcomes are listed as follows:

- when $Nb, Nt,$ M and Ω are increased, $-\theta'(0)$ lowers, whereas λ, α and δ are increased, $-\theta'(0)$ grows.
- $-\theta'(0)$ increases as values of S_r and D_f are increased.
- $C_{fx}(0)$ grows for higher values of D_f. while $-\phi'(0)$ and $C_{fx}(0)$ lowers for higher values of S_r.
- $C_{fx}(0)$ increases as the inclination factor (Ω) increases, but $-\phi'(0)$ and $-\theta'(0)$ decreases.
- Temperature profile and concentration profile has a direct relation against D_f and S_r.

The proposed analysis can be used for more realistic applications in industrial sector. Entropy generation, exothermic endothermic reactive analysis etc. can be considered as a future work.

Nomenclature

Electrical conductivity	σ
Density of fluid	ρ
Components of velocity	u, v
Spin gradient viscosity	γ^*
Vertex viscosity	k_1^*
Micro- inertia per unit mass	j^*
Thermal diffusivity	α
Angle of inclination	Ω
Thermal conductivity	k
Radiation parameter	Rd
Schmidt number	Sc
Thermophoretic diffusion coefficient	D_T
Brownian motion	D_B
Specific heat	c_p
Concentration susceptibility	c_s
Thermal diffusion ratio	K_T
Viscosity	μ
Soret number	Sr
Dufour number	Df
Magnetic effect	M

CRediT authorship contribution statement

Mohammad Mahtab alam: Writing – review & editing. **Ikram Ullah:** Supervision, Investigation. **Ali Hasan Ali:** Visualization. **saira shukat:** Software, Methodology. **Marouan Kouki:** Investigation.

Declaration of Competing Interest

The authors declare that they have no known competing financial interests or personal relationships that could have appeared to influence the work reported in this paper.

Acknowledgements

The authors extend their appreciation to the Deanship of Research and Graduate Studies at King Khalid University for funding this work through Large Research Project under grant number RGP2/525/45. The authors extend their appreciation to the Deanship of Scientific Research at Northern Border University, Arar, KSA for funding this research work through the project number "NBU-FPEJ-2024-2570-05"

References

[1] B.C. Sakiadis, Boundary layer behavior on continuous solid surfaces: I. Boundary layer equations for two-dimensional and axisymmetric flow, AIChE J. 7 (1966) 26–28.
[2] Y.S. Daniel, Z.A. Aziz, Z. Ismail, F. Salah, Impact of thermal radiation on electrical MHD flow of nanofluid over nonlinear stretching sheet with variable thickness, Alex. Eng. J. *57* (3) (2018) 2187–2197.
[3] Y.S. Daniel, Z.A. Aziz, Z. Ismail, F. Salah, Thermal stratification effects on MHD radiative flow of nanofluid over nonlinear stretching sheet with variable thickness, J. Comput. Des. Eng. *5* (2) (2018) 232–242.
[4] A.S. Warke, K. Ramesh, F. Mebarek-Oudina, A. Abidi, Numerical investigation of the stagnation point flow of radiative magnetomicropolar liquid past a heated porous stretching sheet, J. Therm. Anal. Calorim. *147* (12) (2022) 6901–6912.
[5] N. Acharya, Effects of different thermal modes of obstacles on the natural convective Al2O3-water nanofluidic transport inside a triangular cavity, Proc. Inst. Mech. Eng. Part C J. Mech. Eng. Sci. *236* (10) (2022) 5282–5299.
[6] Ullah, Activation energy with exothermic/endothermic reaction and Coriolis force effects on magnetized nanomaterials flow through Darcy–Forchheimer porous space with variable features, Waves Random Complex Media (2022) 1–14.
[7] N. Acharya, Magnetized hybrid nanofluid flow within a cube fitted with circular cylinder and its different thermal boundary conditions, J. Magn. Magn. Mater. *564* (2022) 170167.
[8] N. Acharya, Hydrothermal scenario of buoyancy-driven magnetized multi-walled carbon nanotube-Fe3O4-water hybrid nanofluid flow within a discretely heated circular chamber fitted with fins, J. Magn. Magn. Mater. *589* (2024) 171612.
[9] I. Ullah, Heat transfer enhancement in Marangoni convection and nonlinear radiative flow of gasoline oil conveying Boehmite alumina and aluminum alloy nanoparticles, Int. Commun. Heat. Mass Transf. 132 (2022) 105920.
[10] N. Acharya, Buoyancy driven magnetohydrodynamic hybrid nanofluid flow within a circular enclosure fitted with fins, Int. Commun. Heat. Mass Transf. *133* (2022) 105980.
[11] S. Amin, I. Ullah, S. Shukat, M. Kouki, H. Ahmad, M.M. Alam, H. Khan, Lorentz force and solar energy case study on CNTs and pollytetrafluoroethylene (PTFE) paraffin oil-based hybrid nanofluid flow through a porous divergent/convergent channel, Case Stud. Therm. Eng. *58* (2024) 104378.
[12] N.N. Kumar, D.R.V.S.R.K. Sastry, S. Shaw, Irreversibility analysis of an unsteady micropolar CNT-blood nanofluid flow through a squeezing channel with activation energy-Application in drug delivery, Comput. Methods Prog. Biomed. *226* (2022) 107156.
[13] M.K. Nayak, S. Shaw, H. Waqas, O.D. Makinde, M. Alghamdi, T. Muhammad, Comparative study for magnetized flow of nanofluids between two parallel permeable stretching/shrinking surfaces, Case Stud. Therm. Eng. *28* (2021) 101353.
[14] D.R.V.S.R.K. Sastry, N. Naresh Kumar, S. Shaw, Numerical simulation of unsteady ethylene glycol/CNTs micropolar nanofluid flow through a squeezing channel: an approach to industrial applications, Heat. Transf. *51* (6) (2022) 4906–4928.
[15] M.K. Nayak, S. Shaw, M.I. Khan, V.S. Pandey, M. Nazeer, Flow and thermal analysis on Darcy-Forchheimer flow of copper-water nanofluid due to a rotating disk: a static and dynamic approach, J. Mater. Res. Technol. *9* (4) (2020) 7387–7408.
[16] D. Mohanty, G. Mahanta, S. Shaw, Irreversibility and thermal performance of nonlinear radiative cross-ternary hybrid nanofluid flow about a stretching cylinder with industrial applications, Powder Technol. *433* (2024) 119255.
[17] D. Mohanty, G. Mahanta, S. Shaw, Analysis of irreversibility for 3-D MHD convective Darcy–Forchheimer Casson hybrid nanofluid flow due to a rotating disk with Cattaneo–Christov heat flux, Joule heating, and nonlinear thermal radiation, Numer. Heat. Transf., Part B: Fundam. *84* (2) (2023) 115–142.
[18] I. Ullah, S. Shukat, A. Albakri, H. Khan, A.M. Galal, W. Jamshed, Thermal performance of aqueous alumina–titania hybrid nanomaterials dispersed in rotating channel. Int. J. Mod. Phys. B *37* (24) (2023) 2350237.
[19] P. Mathur, S.R. Mishra, P.K. Pattnaik, R.K. Dash, Characteristics of Darcy–Forchheimer drag coefficients and velocity slip on the flow of micropolar nanofluid. Heat. Transf. *50* (7) (2021) 6529–6547.
[20] S.U.D. Sathyanarayanan, F. Mabood, W. Jamshed, S.R. Mishra, K. Nisar, P. K. Pattnaik, M. Zakarya, Irreversibility process characteristics of variant viscosity and conductivity on hybrid nanofluid flow through Poiseuille microchannel: A special case study, Case Stud. Therm. Eng. *27* (2021) 101337.
[21] B. Mohanty, S. Jena, P.K. Pattnaik, MHD nanofluid flow over stretching/shrinking surface in presence of heat radiation using numerical method, Int. J. Emerg. Technol. *10* (2) (2019) 119–125.
[22] A. Jan, R. Nawaz, A. Ahmad, Non-similar analysis of radially magnetized flow and heat transfer of Reiner–Philippoff based nanofluid over a curved stretching surface with viscous dissipation. Int. J. Thermofluids *22* (2024) 100657.
[23] J. Cui, A. Jan, U. Farooq, M. Hussain, W.A. Khan, Thermal analysis of radiative Darcy–Forchheimer nanofluid flow across an inclined stretching surface. Nanomaterials *12* (23) (2022) 4291.
[24] J. Cui, U. Farooq, A. Jan, M. Hussain, Non-similar bioconvective analysis of magnetized hybrid nanofluid (Ag+ TiO2) flow over exponential stretching surface, Heliyon *10* (9) (2024).
[25] J. Cui, U. Farooq, A. Jan, M.K. Elbashir, W.A. Khan, M. Mohammed, J. Ul Rahman, Significance of nonsimilar numerical simulations in forced convection from stretching cylinder subjected to external magnetized flow of Sisko fluid, J. Math. *2021* (1) (2021) 9540195.
[26] A. Jan, M. Mushtaq, M. Hussain, Heat transfer enhancement of forced convection magnetized cross model ternary hybrid nanofluid flow over a stretching cylinder: non-similar analysis, Int. J. Heat. Fluid Flow. *106* (2024) 109302.
[27] B. Mohanty, S. Mohanty, S.R. Mishra, P.K. Pattnaik, Analysis of entropy on the peristaltic transport of micropolar nanofluid: a simulation obtained using approximate analytical technique, Eur. Phys. J. *136* (2021) 1–19.
[28] P. Mathur, S.R. Mishra, P.K. Pattnaik, R.K. Dash, Characteristics of Darcy–Forchheimer drag coefficients and velocity slip on the flow of micropolar nanofluid. Heat. Transf. *50* (7) (2021) 6529–6547.
[29] B. Mohanty, S. Jena, P.K. Pattnaik, MHD nanofluid flow over stretching/shrinking surface in presence of heat radiation using numerical method, Int. J. Emerg. Technol. *10* (2) (2019) 119–125.
[30] S.R. Mishra, P. Mathur, H.M. Ali, Analysis of homogeneous–heterogeneous reactions in a micropolar nanofluid past a nonlinear stretching surface: semi-analytical approach. J. Therm. Anal. Calorim. *144* (6) (2021) 2247–2257.
[31] P. Mathur, S.R. Mishra, P.K. Pattnaik, R.K. Dash, Characteristics of Darcy–Forchheimer drag coefficients and velocity slip on the flow of micropolar nanofluid. Heat. Transf. *50* (7) (2021) 6529–6547.
[32] S.U. Choi, J.A. Eastman, *Enhancing thermal conductivity of fluids with nanoparticles* (No. ANL/MSD/CP-84938; CONF-951135-29), Argonne National Lab.(ANL), Argonne, IL (United States), 1995.
[33] Buongiorno, J. (2006). Convective transport in nanofluids.
[34] W.A. Khan, I. Pop, "Boundary-layer flow of a nanofluid past a stretching sheet", Int. J. Heat. Mass Transf. 53 (11-12) (2010) 2477–2483.
[35] Z. Alhajaj, A.M. Bayomy, M.Z. Saghir, M.M. Rahman, Flow of nanofluid and hybrid fluid in porous channels: Experimental and numerical approach, Int. J. Thermofluids *1* (2020) 100016.
[36] Jan, Refat Ullah, et al., "Heat transfer analysis in hybrid nano-composite flow in a stretchable convergent/divergent channel in the preaence of Darcy-Forchheimer law and Lorentz force", Ain Shams Eng. J. (2024) 102828.
[37] F. Gamar, M.D. Shamshuddin, M.S. Ram, S.O. Salawu, Arrhenius evaluation of thermal radiative flux and energy for flowing micropolar nanofluid at stagnation point: a case of thermal study, J. Therm. Anal. Calorim. (2024) 1–11.

[38] F. Gamar, M.D. Shamshuddin, M.S. Ram, S.O. Salawu, E.O. Fatunmbi, Exploration of thermal radiation and stagnation point in MHD micropolar nanofluid flow over a stretching sheet with Navier slip, Numer. Heat. Transf., Part A: Appl. (2024) 1–13.
[39] M.D. Shamshuddin, F. Mabood, W.A. Khan, G.R. Rajput, Exploration of thermal Péclet number, vortex viscosity, and Reynolds number on two-dimensional flow of micropolar fluid through a channel due to mixed convection. Heat. Transf. *52* (1) (2023) 854–873.
[40] M.D. Shamshuddin, A. Saeed, S.R. Mishra, R. Katta, M.R. Eid, Homotopic simulation of MHD bioconvective flow of water-based hybrid nanofluid over a thermal convective exponential stretching surface, Int. J. Numer. Methods Heat. Fluid Flow. *34* (1) (2024) 31–53.
[41] A. Farooq, R. Ali, A.C. Benim, Soret and Dufour effects on three dimensional Oldroyd-B fluid, Phys. A: Stat. Mech. its Appl. *503* (2018) 345–354.
[42] T. Hayat, I. Ullah, T. Muhammad, A. Alsaedi, Radiative three-dimensional flow with Soret and Dufour effects, Int. J. Mech. Sci. *133* (2017) 829–837.
[43] H. Sardar, L. Ahmad, M. Khan, A.S. Alshomrani, Investigation of mixed convection flow of Carreau nanofluid over a wedge in the presence of Soret and Dufour effects, Int. J. Heat. Mass Transf. *137* (2019) 809–822.
[44] A. Shojaei, A.J. Amiri, S.S. Ardahaie, K. Hosseinzadeh, D.D. Ganji, Hy9drothermal analysis of Non-Newtonian second grade fluid flow on radiative stretching cylider with Soret and Dufour effects, Case Stud. Therm. Eng. *13* (2019) 100384.
[45] A.F. Al-Mudhaf, A.M. Rashad, S.E. Ahmed, A.J. Chamkha, S.M.M. El-Kabeir, Soret and Dufour effects on unsteady double diffusive natural convection in porous trapezoidal enclosures, Int. J. Mech. Sci. *140* (2018) 172–178.
[46] Y. Meng, B. Li, On viscoelastic fluid in a vertical porous media channel with Soret and Dufour effects, Appl. Math. Lett. *124* (2022) 107656.
[47] M.R. Eid, W. Jamshed, B.S. Goud, R.W. Ibrahim, S.M. El Din, A. Abd-Elmonem, N. S.E. Abdalla, Mathematical analysis for energy transfer of micropolar magnetic viscous nanofluid flow on permeable inclined surface and Dufour impact, Case Stud. Therm. Eng. *49* (2023) 103296.
[48] F. Shah, T. Hayat, S. Momani, Non-similar analysis of the Cattaneo-Christov model in MHD second-grade nanofluid flow with Soret and Dufour effects, Alex. Eng. J. *70* (2023) 25–35.
[49] K. Borah, J. Konch, S. Chakraborty, SORET AND DUFOUR EFFECTS ON MHD FLOW OF A MICROPOLAR FLUID PAST OVER A VERTICAL RIGA PLATE, J. Appl. Math. Comput. Mech. *22* (3) (2023).
[50] K. Sudarmozhi, D. Iranian, I. Khan, S. Al-Otaibi, EFFECTS OF POROUS MEDIUM IN MHD FLOW OF MAXWELL FLUID WITH SORET/DUFOUR IMPACTS, J. Porous Media *27* (2024).
[51] G.S. Mini, P.V. Kumar, S.M. Ibrahim, Numerical Computation of Radiative MHD Micropolar Nanofluid Flow over a Stretching Sheet with First Order Chemical Reaction and Soret Effects, J. Adv. Res. Fluid Mech. Therm. Sci. *108* (2) (2023) 77–97.
[52] G. Revathi, K.R. Gujjula, M. Jayachandra Babu, Influence of shape factor on a chemically reactive hybrid nanofluid flow via a moving plate when Soret and Dufour effects are significant: An irreversibility analysis with Cattaneo-Christov heat flux model, Numer. Heat. Transf., Part A: Appl. (2023) 1–19.
[53] S.L. Sun, D. Liu, Y.Z. Wang, Y.L. Qi, H.B. Kim, Heat transportation performance and entropy generation analysis of Iron (II, III) oxide microparticles on Taylor Couette flow over a slit wall, Int. Commun. Heat. Mass Transf. *139* (2022) 106479.
[54] S.L. Sun, D. Liu, Y.Z. Wang, Y.L. Qi, H.B. Kim, Convective heat transfer and entropy generation evaluation in the Taylor–Couette flow under the magnetic field. Int. J. Mech. Sci. *252* (2023) 108373.
[55] H. Waqas, U. Farooq, D. Liu, M. Abid, M. Imran, T. Muhammad, Heat transfer analysis of hybrid nanofluid flow with thermal radiation through a stretching sheet: A comparative study, Int. Commun. Heat. Mass Transf. *138* (2022) 106303.
[56] B. Ahmed, D. Liu, Y. Zhang, M.A. Hussien, Peristaltic pumping of convective nanofluid with magnetic field and thermal radiation in a porous channel, Case Stud. Therm. Eng. *53* (2024) 103918.
[57] B. Bidin, R. Nazar, Numerical solution of the boundary layer flow over an exponentially stretching sheet with thermal radiation, Eur. J. Sci. Res. *33* (4) (2009) 710–717.
[58] A. Ishak, MHD boundary layer flow due to an exponentially stretching sheet with radiation effect, Sains Malays. *40* (4) (2011) 391–395.